Suppression of laser beam's polarization and intensity fluctuation via a Mach–Zehnder interferometer with proper feedback

View Online   Export Citation   CrossMark

Xiaokai Hou,[1] (iD) Shuo Liu,[1,a] (iD) Xin Wang,[1] Feifei Lu,[1] Jun He,[1,2] and Junmin Wang[1,2,b] (iD)

AFFILIATIONS

[1] State Key Laboratory of Quantum Optics and Quantum Optics Devices, and Institute of Opto-Electronics, Shanxi University, Tai Yuan 030006 Shanxi Province, China

[2] Collaborative Innovation Center of Extreme Optics, Shanxi University, Tai Yuan 030006 Shanxi Province, China

[a] Present address: Key Laboratory of Laser and Infrared System of Ministry of Education, Shandong University, Qing Dao 266000, Shandong Province, China.
[b] Author to whom correspondence should be addressed: wwjjmm@sxu.edu.cn

ABSTRACT

Long ground-Rydberg coherence lifetime is interesting for implementing high-fidelity quantum logic gates, many-body physics, and other quantum information protocols. However, the potential well formed by a conventional far-off-resonance red-detuned optical-dipole trap that is attractive for ground-state cold atoms is usually repulsive for Rydberg atoms, which will result in the rapid loss of atoms and low repetition rate of the experimental sequence. Moreover, the coherence time will be sharply shortened due to the residual thermal motion of cold atoms. These issues can be addressed by a one-dimensional magic lattice trap, which can form a deeper potential trap than the traveling wave optical dipole trap when the output power is limited. In addition, these common techniques for atomic confinement generally have certain requirements for the polarization and intensity stability of the laser. Here, we demonstrated a method to suppress both the polarization drift and power fluctuation only based on the phase management of the Mach–Zehnder interferometer for a one-dimensional magic lattice trap. With the combination of three wave plates and the interferometer, we used the instrument to collect data in the time domain, analyzed the fluctuation of laser intensity, and calculated the noise power spectral density. We found that the total intensity fluctuation comprising laser power fluctuation and polarization drift was significantly suppressed, and the noise power spectral density after closed-loop locking with a typical bandwidth of 1–3000 Hz was significantly lower than that under the free running of the laser system. Typically, at 1000 Hz, the noise power spectral density after locking was about 10 dB lower than that under the free running of a master oscillator power amplifier system. The intensity–polarization control technique provides potential applications for atomic confinement protocols that demand fixed polarization and intensity.

I. INTRODUCTION

For various atomic manipulation experiments, such as single photon source,[1–5] quantum dynamics based on Rydberg states,[6–10] and electric field detection based on atoms,[11–13] strong confinement optical dipole trap (ODT) of atoms is usually employed. In these applications, a high-power laser with fixed polarization and relatively stabled intensity is normally used to confine atoms. The common experimental setup for the laser power stabilization was based on the active feedback loop, which used an acousto-optic modulator (AOM)[14–17] or an electro-optic modulator (EOM)[18] as the actuator. In 2020, AOM and EOM were combined to broaden the bandwidth of laser intensity noise stabilization to 1 MHz by Ni *et al.*[19] Currently, the feedback loop based on AOM has some disadvantages. For example, the Bragg diffraction of AOM will seriously affect the spot quality of first-order diffraction light, and the power utilization of the system will be limited by the diffraction efficiency of the AOM. The common electro-optic intensity modulator

(EOIM) with input and output tailed fiber is efficient but is not suitable for high-power applications. Moreover, the above-mentioned schemes can observably suppress the power fluctuation of the laser beam, but the reduction of the drift of the laser's polarization is still not effectively achieved. Here, we demonstrate an experimental scheme based on the Mach–Zehnder interferometer (MZI) for actively suppressing both the fluctuation of power and polarization of the laser beam. By properly manipulating the phase difference between the two paths, it is observed that the output fraction of the MZI accounts for the majority of laser power, while its intensity fluctuation in the time domain has been reduced dozens of times compared with the free-running case, and the noise power spectral density (NPSD) has been decreased in the range of 1–3000 Hz in the frequency domain. Such a stable system can certainly meet the needs of various applications, such as experiments where the lifetime of cold atoms is highly desirable.

II. THEORETICAL BACKGROUND

A. Magic optical dipole trap for cesium $6S_{1/2}$ ground state and $84P_{3/2}$ Rydberg state

Recently, a new experimental scheme, which used an interferometer as the actuator of the feedback loop, has been proposed.[20] Considering the light intensity requirement of the ODT, the MZI can satisfy the power requirement of the ODT without affecting the spot quality of the output light. Therefore, the experimental setups for constructing the blue-detuning optical trap reported by Yelin et al.[21] and Isenhower et al.[22] both concentrate on the MZI. The intensity of the output laser mainly depends on the phase difference between the two arms of the MZI; therefore, it can be used as a power stabilizer in some experiments.[23] Due to the particularity of the output fraction of the MZI, the combination of interferometer and polarizer can realize fixed polarization, high proportion output, and high-intensity stability. It is obviously useful for the experiment of the optical trap. The potential of ODT U can be expressed as

$$U = -\frac{\alpha}{2\varepsilon_0 c} \frac{2P}{\pi \omega_0^2}, \tag{1}$$

where α is the induced polarizability of the target state, ε_0 is the permittivity of vacuum, c is the speed of light, P is the intensity of the laser, and ω_0 is the radius of the spot at the focal point after the laser is focused by a lens. As shown in Eq. (1), if the power of the 1879 nm laser is fluctuant, the resulting trap depth will be changed. Thus, the lifetime of the trapped atom will be severely affected by the presence of the heating mechanism.[5,17,24]

In most of the experiments of cold atoms involving confinement of ground-state atoms in an ODT and Rydberg excitation, the cold atomic sample is prepared in an ODT to hold them in a fixed position for a significantly long time. The potential formed by a conventional far off-resonance red-detuned ODT is attractive for the ground-state atoms, but is usually repulsive for highly excited Rydberg atoms, meaning that Rydberg atoms normally cannot be confined in the conventional ODT [Fig. 1(a)]. Therefore, in the follow-up experiments, we will face the following two problems: (1) if the ODT is switched off during Rydberg excitation and coherent manipulation, it will result in atomic dephasing due to the thermal diffusion of the atoms and the extremely low repetition rate of the
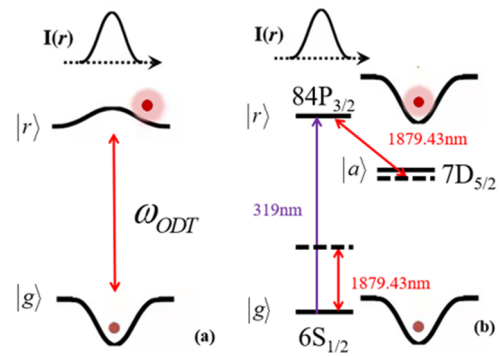

FIG. 1. Diagram of the light shift induced by the ODT and MODT. The intensity of the laser, which is intensely focused, is still Gaussian, and the closer to the center of the beam, the stronger the intensity of the laser. The resulting trap depth or light shift is spatially dependent. (a) The ODT is attractive for ground states but is usually repulsive for highly excited Rydberg states because almost all strong dipole transitions connected the Rydberg state and the lower states have a longer wavelength than that of the ODT laser. (b) The direct single-photon excitation scheme from cesium $|g\rangle = |6S_{1/2}\rangle$ to $|r\rangle = |84P_{3/2}\rangle$ coupled by a 319 nm ultraviolet laser. A 1879.43 nm laser is also tuned to the blue side of the $|r\rangle \Longleftrightarrow |a\rangle = |7D_{5/2}\rangle$ auxiliary transition to equalize the trapping potential depth of the $|g\rangle$ and $|r\rangle$ states, which is the so-called magic ODT (MODT).

experimental sequence; (2) if the ODT remains in operation, it may lower the Rydberg excitation efficiency of atoms as the transition frequency is spatially position-dependent on the excitation laser. The solution is to find an ODT such that the ground-state atoms and the desired highly excited Rydberg atoms can experience the same potential, i.e., the potential generated by the ODT is a potential well for both the ground-state atoms and the desired highly excited Rydberg atoms, and is attractive to atoms in both states. Therefore, the above-mentioned aspects (1) and (2) can be solved. In Fig. 1(b), the direct single-photon excitation scheme from cesium $|g\rangle = |6S_{1/2}\rangle$ to $|r\rangle = |84P_{3/2}\rangle$ coupled by a 319 nm ultraviolet laser. A 1879.43 nm laser is also tuned to the blue side of the $|r\rangle \Longleftrightarrow |a\rangle = |7D_{5/2}\rangle$ auxiliary transition to equalize the trapping potential depth of the $|g\rangle$ and $|r\rangle$ states. The specific calculation process is not described here. For details, please refer to Refs. 25 and 26.

B. Theoretical analysis of MZI

The MODT is not enough to meet the need for extremely long coherence time in subsequent experiments. The cold atoms trapped in the MODT still have residual thermal motion, which causes violent collisions that heat the atoms and cause them to escape from the trap. We will further construct a one-dimensional magic lattice trap (1D-MLT), and combine the advantages of lattice and magic conditions, in order to prolong the coherence time of the ground-Rydberg state of cold atoms. The 1D-MLT also needs to suppress its power fluctuation. Because the power of the laser used in the 1D-MLT fluctuates in the time domain, we will directly shorten the coherence lifetime of the cold atom. Therefore, we use the MZI to suppress the power fluctuation.

As shown in Fig. 2(a), I_{out1} and I_{out2} are the intensities of two output paths of the interferometer; R_1 and R_2, and T_1 and T_2 are the reflectivity and transmittance of input and output beam splitters
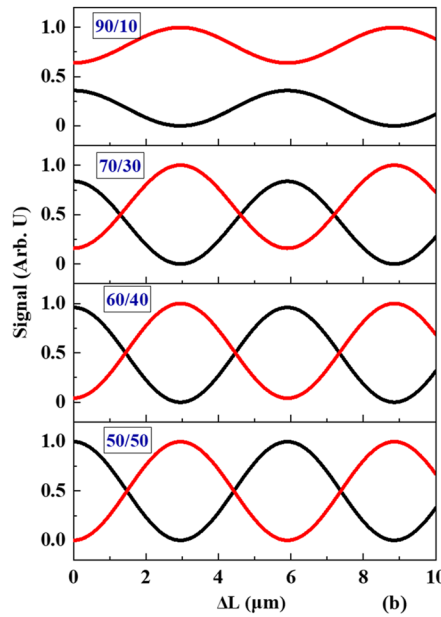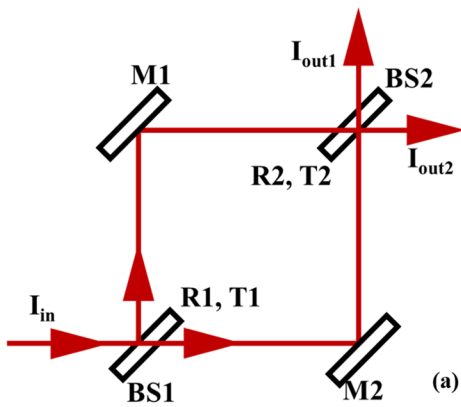
FIG. 2. Diagrams of MZI and interference fringes of two channels of the MZI that are simulated and analyzed theoretically. (a) MZI consists of two beam splitter plates (BS1 and BS2) and two high-reflectivity mirrors (M1 and M2). I_{in} is the intensity of the incident light field, and I_{out1} and I_{out2} are the intensities of the outgoing light field at BS2. (b) Normalized signal as a function of the difference of optical path ΔL for different splitter ratios. This ratio is both R_1/T_1 and R_2/T_2 because BS1 and BS2 used in the MZI are the same. The solid red and black lines represent the interference fringes of the two output channels of MZI.

plates, respectively. The two output channels of the interferometer can be expressed as follows:

$$I_{out1} = R_1^2 R_2^2 + T_1^2 T_2^2 + 2R_1 R_2 T_1 T_2 \cos\left(\frac{2\Delta L}{\lambda} + \pi\right), \quad (2)$$

$$I_{out2} = R_1^2 R_2^2 + T_1^2 T_2^2 + 2R_1 R_2 T_1 T_2 \cos\left(\frac{2\Delta L}{\lambda}\right). \quad (3)$$

Therefore, the laser intensity output of the interferometer can be controlled by adjusting the driving voltage of the piezoelectric transducer (PZT) due to the correlation between the output transmittance I and the optical path difference ΔL. In Fig. 2(b), the interference fringes generated by splitters with different splitter ratios are simulated and analyzed using Mathematica. In Fig. 2(b), the splitter ratio shown by the first line pattern is 90/10, the second is 70/30, the third is 60/40, and the fourth is 50/50.

III. EXPERIMENTAL SETUP

The laser intensity stabilization setup is shown in Fig. 3. A master oscillator power amplifier (MOPA) system consists of a 1879-nm butterfly packaged laser diode and a thulium-doped fiber amplifier (TmDFA), which has a maximum output of ~3 W. With a free space polarization controller based on three waveplates ($\lambda/4$, $\lambda/2$, and $\lambda/4$), polarization fluctuation of 1879 nm beam is suppressed initially. The
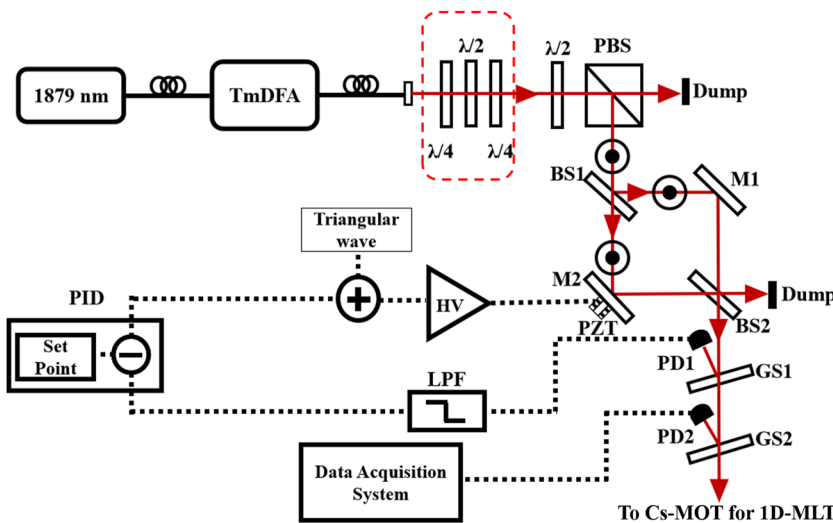
FIG. 3. Experimental setup for the intensity stabilization system. The dynamic stability of the laser intensity of the 1879 nm MOPA system is realized by the MZI, and the fluctuation of the laser intensity is monitored and analyzed in the time and frequency domains. $\lambda/2$: half-wave plate; $\lambda/4$: quarter-wave plate; PBS: polarization beam splitting cube; BS: beam splitting plate; GS: glass slice; M1/M2: high-reflectivity mirror; PD: photodetector; LPF: low-pass filter; PID: proportional integral differential amplifier; HVA: high voltage amplifier.

laser is injected into an MZI that is constructed by using a 50/50 beam splitter plate (BS1) that divides the incident light into two beams with equal intensity and different phases, a high-reflectivity mirror (M1) that reflects one beam, a mirror (M2) attached to a PZT that emits the other beam, and a beam splitter plate (BS2) that finally combines the two beams. The interferometer has two output channels, where each channel can be used for dynamic feedback to make the system more stable and the output of this channel can then be used for subsequent experiments. The photodetector (PD1) is mounted behind a glass slice (GS1) of 1879 nm for sampling a small fraction of light for in-loop feedback. The DC voltage signal output by the PD1 is injected into a proportional integral differential (PID) amplifier after passing through a low-pass filter (LPF). The input signal of the PID controller is subtracted from the PID set point, which is an artificially set reference DC voltage. The output signal of PID, i.e., the real-time difference between the detector signal and the reference DC voltage, is added with the scanning signal (triangular wave) and amplified by the high voltage (HV) amplifier as the driving voltage of the PZT. Therefore, the output power of the interferometer can be controlled by manipulating the driving voltage of the PZT, and we expect that both the power and polarization fluctuations for the 1879 nm laser are suppressed. In addition, another photodetector (PD2) is mounted in order to independently monitor the intensity stability of the output linear polarization laser. The output signal of PD2 is then injected into the data acquisition system (Keithley, DAQ-6510) in order to analyze and monitor the intensity fluctuation of the laser in the time domain, and calculate the NPSD based on the measured optical power fluctuation data. Undoubtedly, a small fraction of the far-infrared laser is reflected by the glass slice (GS2) and received by the PD2, and the majority of the laser is transmitted and focused in a cesium magneto-optical trap (Cs-MOT) for the construction of the ODT.
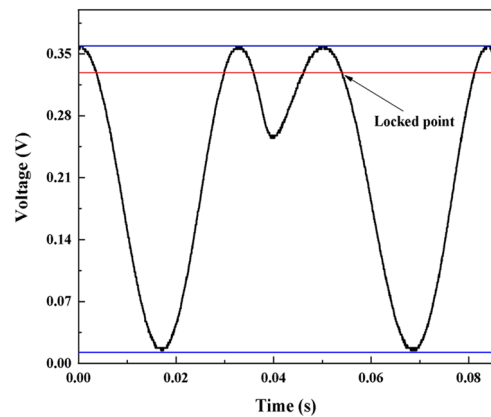

FIG. 4. Interference fringe of the MZI. In the experiment, a 50/50 beam splitter plate is used, and the PZT is driven by scanning triangular wave so that the phase difference between the two arms is generated and then the interference fringes are generated.

IV. EXPERIMENTAL RESULTS AND DISCUSSION

Figure 4 shows the interference fringes obtained by scanning triangular waves with a 50/50 beam splitter ratio in the experiment, in which the interference contrast is 95%. In the theoretical simulation, an interference fringe with an interference contrast of 99.9% can be obtained by using a 50/50 beam splitter plate; however, the best interference contrast is not achieved in the experiment probably due to the following two reasons: first, the spatial mode of the two lasers is not exactly same; second, the polarization of the two lasers may be slightly different.
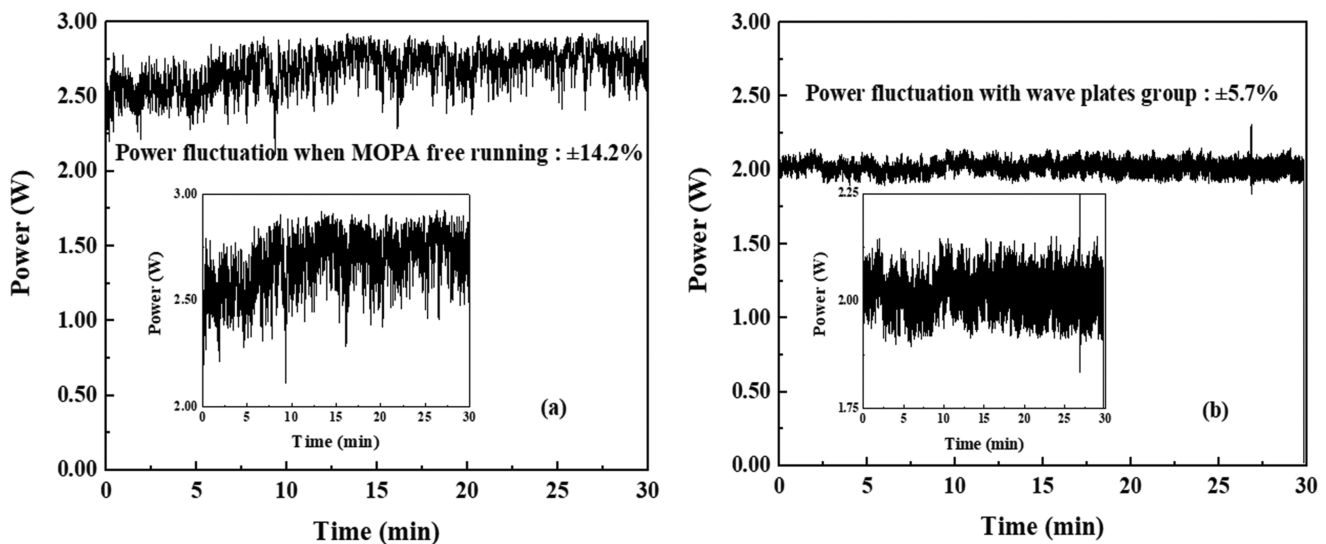

FIG. 5. (a) The power fluctuation of free running 1879 nm MOPA system. Through 30 min of measurement, the power fluctuation is roughly ±14.2%. The inset is zoomed in on the vertical axis from 2.00 to 3.00 W and shows the intensity fluctuation in 30 min. (b) The power fluctuation after three wave plates. We thought that the polarization fluctuation is initially suppressed by these plates. Similarly, after 30 min of measurement, the intensity fluctuation is roughly ± 5.7%. Furthermore, the vertical axis range of the inset becomes 1.75–2.25 W, and the range of the horizontal axis is still 0–30 min.
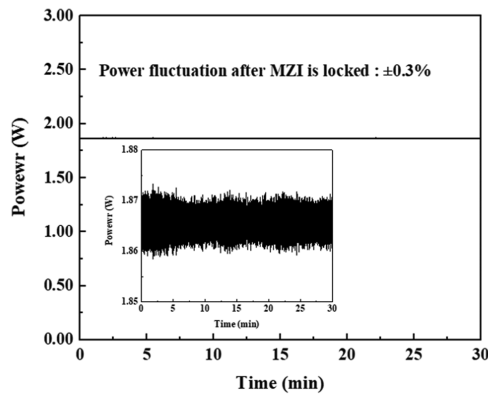
FIG. 6. The intensity fluctuation of the 1879 nm laser on the bright fringe of the MZI. By closed-loop locking, the phase difference between the two arms is dynamically compensated, and the power fluctuation is significantly suppressed; through 30 min of measurement, the power fluctuation is roughly ±0.3%. The vertical axis of the inset has been enlarged with a range of 1.85–1.88 W and shows the 30-min measurement.

Considering the requirement of constructing a dipole trap with this laser source, the polarization of the 1879 nm laser should be fixed. Therefore, the PBS is usually inserted in the light path to fix the polarization of light. Even though the scheme is effective, an inevitable defect existing in this scheme is that the polarization fluctuation of light will couple with the intensity fluctuation through this polarization element. As the measurement of the intensity for 1879 nm laser after PBS, although the power fluctuation of 1879 nm TmDFA itself is not obvious, the intensity fluctuation behind the PBS becomes obvious, and the results are shown in Fig. 5(a). We monitor the laser intensity for about 30 min in the time domain, with a large fluctuation of about ±14.2%. The huge intensity fluctuation will significantly affect the power utilization of the stable system. To maximize power utilization, three wave plates are used to initially suppress the power fluctuation. After proper adjustment, the measurement result of laser intensity fluctuation after PBS is shown in Fig. 5(b). The fluctuation of laser polarization has been reduced significantly. Then, the initially stabled laser has been injected in the combined system of MZI and another PBS, where the transmittance of the interferometer is locked up to 90% in order to improve power utilization. Then, the intensity fluctuation probed by the out-of-loop detector PD2 is shown in Fig. 6. As shown in Fig. 6, the intensity fluctuation of the output linearly polarized laser is reduced to

±0.3%, which is much better than the fluctuation of direct TmDFA-PBS output. At this stability, both the fluctuation of the laser power and polarization will no longer have a significant influence on the parameter of the dipole trap.

As shown in Table I, for the 1879 nm 1D-MLT, if the laser is focused through a lens to ~20 μm and the incident laser power at the cold atom is about 1.5 W, the maximum depth of the 1D-MLT is −1000 μK and the typical trap depth fluctuation is ±140 μK. When the laser power decreases after the initial suppression of the wave plate group or the closed-loop locking of the MZI, the corresponding typical trap depth is about −800 and −700 μK. In addition, the effective temperature of the cold atoms, which are transferred from MOT to 1D-MLT, will be slightly higher, about 100 μK; on the other hand, the decrease in the trap depth caused by the suppression of the power fluctuation will not affect the capture of the cold atoms. However, the residual fluctuation of laser power still exists, which will lead to the typical trap depth fluctuation of ±45 and ±2 μK, respectively.

The collected time-domain voltage signals are used to calculate the NPSD. As shown in Fig. 7, the horizontal range is determined by the sampling rate. In the experiment, we selected a sampling rate of 10 000 Hz according to the actual situation, so the horizontal axis in Fig. 7 ranges from 1 to 5000 Hz. In addition, we believe that the feedback bandwidth of the system should be at the level of kilohertz due to the limitation of PZT in the MZI. Therefore, the sampling rate can fully meet the requirement of representing the feedback bandwidth of the system.

The NPSD after closed-loop locking from 1 to 3000 Hz is significantly lower than that under the free running of the MOPA system. It can be proved that the MZI plays an obvious role in the power stability of the system. To further broaden the feedback bandwidth and improve the inhibitory effect, we assume that the arm length of the MZI is L and the angular frequency of the laser is ω_0. Then, the distance of the laser going through the MZI is L and the phase shift generated is[27]

$$\Phi_0(t) = \omega_0 t = \omega_0 \frac{L}{c}. \tag{4}$$

Here, Φ_0 is a constant and the magnitude is proportional to L. When the PZT is scanned, we begin to characterize small changes in phase. For simplicity, we assume that a sine wave is used to scan the PZT for which the amplitude is h_0 and the angular frequency is ω_s. Therefore, the sine wave can be expressed as

$$h(t) = h_0 \cos(\omega_s t). \tag{5}$$

TABLE I. The typical maximum trap depth and fluctuation of 1879.43 nm 1D-MLT for cesium atoms under different power fluctuations are calculated.

| Category	P_{ODT} (mW)	ΔP (mW)	Gaussian radius after focused (μm)	U_{dip} (μK)	ΔU_{dip} (μK)
MOPA free running	1500	±213.0 (±14.2%)	20	−1000	±140
With wave plate group	1200	±68.4 (±5.7%)	20	−800	±45
After MZI is locked	1100	±3.3 (±0.3%)	20	−700	±2
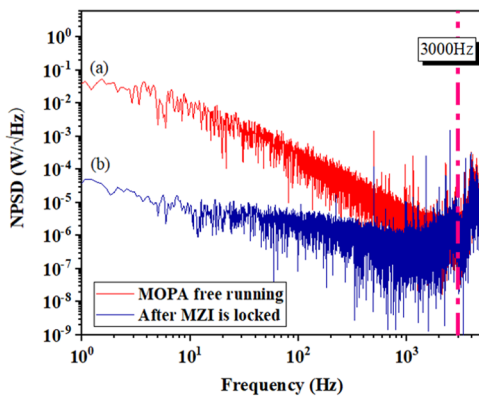
FIG. 7. Intensity noise of the 1879 nm laser as a function of analyzing frequency. (a) The solid black line represents the NPSD when the 1879 nm laser system is running freely without passing through the wave plate group. (b) The solid blue line represents the NPSD of the 1879 nm laser system after closed-loop locking by the MZI.

Hence, the phase shift of the entire system can be written as

$$
\begin{aligned}
\Phi &= \Phi_0(t) + \delta\phi \\
&= \frac{\omega_0 L}{c} + \frac{\omega_0}{2} \int_{t-\frac{L}{c}}^{t} h_0 \, \cos(\omega_s t) dt \\
&= \frac{\omega_0 L}{c} + \frac{h_0}{2}\frac{\omega_0}{\omega_s}\left\{ \sin\left(\omega_s \frac{L}{c}\right) - \sin\left[\omega_s\left(t - \frac{L}{c}\right)\right]\right\} \\
&= \frac{\omega_0 L}{c} + h_0 \frac{\omega_0}{\omega_s} \sin\left(\omega_s \frac{L}{2c}\right) \cos\left[\frac{\omega_s}{2}\left(t - \frac{L}{c}\right)\right] \quad (6)
\end{aligned}
$$

because $\frac{L}{2c} \ll 1$,

$$
h_0 \frac{\omega_0}{\omega_s} \sin\left(\omega_s \frac{L}{2c}\right) = \frac{h_0 \omega_0}{2}\frac{L}{c}, \quad (7)
$$

$$
\delta\phi \sim \frac{h_0 \omega_0}{2}\frac{L}{c}. \quad (8)
$$

As shown in Eq. (8), if the arm length L of the MZI is increased, $\delta\phi$ of the system can be increased. Thus, the detection sensitivity of the system can be improved and the detection effect of the MZI for phase can be better. Increasing the arm length of the MZI will cause extra noise due to the insufficient stability of the system.

However, such noise can be solved through the isolation platform and system temperature control. We can add an F–P cavity on the two arms of the MZI. The F–P cavity can fold up the optical path, greatly increase the distance of the light in the MZI, and does not need to occupy a large area.

V. CONCLUSIONS

In summary, we have demonstrated the reduction of the power and polarization fluctuation for a 1879 nm laser based on the cooperation of three wave plates and an MZI. The intensity fluctuation is ±14.2% after the combination of the MOPA system and PBS is reduced to ±0.3% with locked MZI. In addition, after MZI is locked, the NPSD is lower than that under free running in the range of

1–3000 Hz. Typically, at 1000 Hz, the NPSD after MZI is locked, which is about 10 dB lower than that when MOPA is free running. The system can not only withstand high power injecting laser but also can stabilize both power and polarization fluctuations without affecting the quality of the light beam for the low-loss output light. The laser power utilizing efficiency can be further improved by improving the transmittance of the locked interferometer or improving the interference visibility.

It is expected that Rydberg atoms can have a long coherence lifetime in subsequent experiments involving the Rydberg dressed ground state. On the one hand, we can use the 1879 nm MOPA system to implement a 1D-MLT, which can both eliminate the position-dependent light shift to capture Rydberg state atoms in optical tweezer like the ground-state atoms and attenuate collisions between cold atoms caused by residual thermal motion to prolong the coherence time of Rydberg atoms. On the other hand, we propose an upgraded interferometer, i.e., adding an F–P cavity to each arm of the interferometer, and using the reflection of the beam in the cavity, the arm length can be extended at least dozens of times, to improve the phase measurement sensitivity of the interferometer and improve the power stability.

AUTHOR DECLARATIONS

Conflict of Interest

The authors have no conflicts to disclose.

Author Contributions

Xiaokai Hou: Data curation (equal); Formal analysis (equal); Software (equal); Writing – original draft (equal). **Shuo Liu**: Data curation (equal); Formal analysis (equal). **Xin Wang**: Data curation (equal); Writing – review & editing (equal). **Feifei Lu**: Formal analysis (equal); Software (equal); Writing – review & editing (equal). **Jun He**: Writing – review & editing (equal). **Junmin Wang**: Supervision (equal); Writing – review & editing (equal).

DATA AVAILABILITY

The data that support the findings of this study are available from the corresponding author upon reasonable request.

REFERENCES

[1] M. Endres, H. Bernien, A. Keesling, H. Levine, E. R. Anschuetz, A. Krajenbrink, C. Senko, V. Vuletic, M. Greiner, and M. D. Lukin, "Atom-by-atom assembly of defect-free one-dimensional cold atom arrays," Science **354**, 1024 (2016).
[2] H. Kim, W. Lee, H.-G. Lee, H. Jo, Y. H. Song, and J. Ahn, "*In situ* single-atom array synthesis using dynamic holographic optical tweezers," Nat. Commun. **7**, 13317 (2016).

[3]B. Darquié, M. P. A. Jones, J. Dingjan, J. Beugnon, S. Bergamini, Y. Sortais, G. Messin, A. Browaeys, and P. Grangier, "Controlled single-photon emission from a single trapped two-level atom," Science **309**, 454–456 (2005).

[4]V. Leong, S. Kosen, B. Srivathsan, G. K. Gulati, A. Cere, and C. Kurtsiefer, "Hong-Ou-Mandel interference between triggered and heralded single photons from separate atomic systems," Phys. Rev. A **91**, 063829 (2015).

[5]B. Liu, G. Jin, J. He, and J. M. Wang, "Suppression of single-cesium-atom heating in a microscopic optical dipole trap for demonstration of an 852-nm triggered single-photon source," Phys. Rev. A **94**, 013409 (2016).

[6]Y. O. Dudin and A. Kuzmich, "Strongly interacting Rydberg excitations of a cold atomic gas," Science **336**, 887–889 (2012).

[7]Y.-Y. Jau, A. M. Hankin, T. Keating, I. H. Deutsch, and G. W. Biedermann, "Entangling atomic spins with a Rydberg-dressed spin-flip blockade," Nat. Phys. **12**, 71–74 (2016).

[8]E. Urban, T. A. Johnson, T. Henage, L. Isenhower, D. D. Yavuz, T. G. Walker, and M. Saffman, "Observation of Rydberg blockade between two atoms," Nat. Phys. **5**, 110–114 (2009).

[9]B. Zhao, M. Müller, K. Hammerer, and P. Zoller, "Efficient quantum repeater based on deterministic Rydberg gates," Phys. Rev. A **81**, 052329 (2010).

[10]A. D. Bounds, N. C. Jackson, R. K. Hanley, R. Faoro, E. M. Bridge, P. Huillery, and M. P. A. Jones, "Rydberg-dressed magneto-optical trap," Phys. Rev. Lett. **120**, 183401 (2018).

[11]J. D. Carter, O. Cherry, and J. D. D. Martin, "Electric-field sensing near the surface microstructure of an atom chip using cold Rydberg atoms," Phys. Rev. A **86**, 053401 (2012).

[12]L. A. Jones, J. D. Carter, and J. D. D. Martin, "Rydberg atoms with a reduced sensitivity to dc and low-frequency electric fields," Phys. Rev. A **87**, 023423 (2013).

[13]J. D. Bai, S. Liu, J. Y. Wang, J. He, and J. M. Wang, "Single-photon Rydberg excitation and trap-loss spectroscopy of cold cesium atoms in a magneto-optical trap by using of a 319-nm ultraviolet laser system," IEEE J. Sel. Top. Quantum Electron. **26**, 1600106 (2020).

[14]J. Junker, P. Oppermann, and B. Willke, "Shot-noise-limited laser power stabilization for the AEI 10 m Prototype interferometer," Opt. Lett. **42**, 755 (2017).

[15]F. Seifert, P. Kwee, M. Heurs, B. Willke, and K. Danzmann, "Laser power stabilization for second-generation gravitational wave detectors," Opt. Lett. **31**, 2000–2002 (2006).

[16]J. J. Du, W. F. Li, G. Li, J. M. Wang, and T. C. Zhang, "Intensity noise suppression of light field by optoelectronic feedback," Optik **124**, 3443–3445 (2013).

[17]R. Sun, X. Wang, K. Zhang, J. He, and J. M. Wang, "Influence of laser intensity fluctuation on single-cesium atom trapping lifetime in a 1064-nm microscopic optical tweezer," Appl. Sci. **10**, 659 (2020).

[18]P. Kwee, B. Willke, and K. Danzmann, "Shot-noise-limited laser power stabilization with a high-power photodiode array," Opt. Lett. **34**, 2912–2914 (2009).

[19]Y. Wang, K. Wang, E. F. Fenton, Y.-W. Lin, K.-K. Ni, and J. D. Hood, "Reduction of laser intensity noise over 1 MHz band for single atom trapping," Opt. Express **28**, 31209 (2020).

[20]S. Inoue and Y. Yamamoto, "Longitudinal-mode-partition noise in a semiconductor-laser-based interferometer," Opt. Lett. **22**, 328–330 (1997).

[21]D. Yelin, B. E. Bouma, and G. J. Tearney, "Generating an adjustable three-dimensional dark focus," Opt. Lett. **29**, 661–663 (2004).

[22]L. Isenhower, W. Williams, A. Dally, and M. Saffman, "Atom trapping in an interferometrically generated bottle beam trap," Opt. Lett. **34**, 1159–1161 (2009).

[23]Y. H. Gao, Y. J. Li, J. X. Feng, and K. S. Zhang, "Stable continuous-wave single-frequency intracavity frequency-doubled laser with intensity noise suppressed in audio frequency region," Chin. Phys. B **28**, 094204 (2019).

[24]T. A. Savard, K. M. O'Hara, and J. E. Thomas, "Laser-noise-induced heating in far-off resonance optical traps," Phys. Rev. A **56**, R1095 (1997).

[25]J. D. Bai, S. Liu, J. He, and J. M. Wang, "Towards implementation of a magic optical-dipole trap for confining ground-state and Rydberg-state cesium cold atoms," J. Phys. B: At., Mol. Opt. Phys. **53**, 155302 (2020).

[26]J. D. Bai, X. Wang, X. K. Hou, W. Y. Liu, and J. M. Wang, "Angle-dependent magic optical trap for the $6S_{1/2} \leftrightarrow nP_{3/2}$ Rydberg transition of cesium atoms," Photonics **9**, 303 (2022).

[27]Y. Y. Wang, X. J. Zhu, J. Liu, Y. B. Ma, Z. H. Zhu, J. W. Cao, Z. H. Du, X. G. Wang, J. Qian, C. Yin, Z. Y. Liu, D. Blair, L. Ju, and C. N. Zhao, "The laser interferometer gravitational wave detector," Prog. Astron. **32**, 348 (2014).